Development of an Adaptive Bypass Element for Passive Entrainment Flow Control in Dry Powder Inhalers

Journal:	*Part C: Journal of Mechanical Engineering Science*
Manuscript ID	JMES-18-0350.R1
Manuscript Type:	Original article
Date Submitted by the Author:	n/a

Complete List of Authors:	Kopsch, Thomas; University of Cambridge Department of Engineering Murnane, Darragh; University of Hertfordshire, Department of Pharmacy, Pharmacology and Postgraduate Medicine Symons, Digby D; University of Canterbury, Mechanical Engineering

Keywords:	Bypass, Optimization, Flow Control, Entrainment, Dry Powder Inhaler

Abstract:	The release of drug from dry powder inhalers (DPIs) is strongly dependent on the patient's inhalation profile. To maximize the effect of the treatment it is necessary to optimize DPIs to achieve drug delivery that (A) is independent of the inhalation manoeuvre and (B) is targeted to the correct site in the lung. The purpose of this study is to develop a DPI with an adaptive bypass element that achieves desired drug delivery behaviour. Computational and experimental methods are used. First, the effect of a generic variable bypass element on entrainment behaviour is modelled. This is done by modelling a DPI as a network of flow. Second, the behaviour of a potential variable bypass element, a flap valve, is studied both computationally and experimentally. Third, the flow resistances are optimized to achieve consistent and desired entrainment behaviour for patients with very different inhalation manoeuvres. A simulated DPI device design was found that achieves an approximately constant entrainment flow rate of 12 L/min when total flow rates larger than 20 L/min are applied. The developed DPI is predicted to accurately deliver drug for patients with highly different inhalation manoeuvres.

Original Article

Corresponding Author:
Thomas Kopsch, Department of Engineering (University of Cambridge), Trumpington Street, CB2 1PZ United Kingdom
Email: Thomas.Kopsch@htwg-konstanz.de

Development of an Adaptive Bypass Element for Passive Entrainment Flow Control in Dry Powder Inhalers

Thomas Kopsch*, Darragh Murnane**, and Digby Symons***

*University of Cambridge, Department of Engineering, Trumpington Street, CB2 1PZ, UK

**University of Hertfordshire, Department of Pharmacy, Pharmacology and Postgraduate Medicine, College Lane, AL10 9AB, UK

***University of Canterbury, Mechanical Engineering Department, Christchurch 8140, New Zealand

Abstract

The release of drug from dry powder inhalers (DPIs) is strongly dependent on the patient's inhalation profile. To maximize the effect of the treatment it is necessary to optimize DPIs to achieve drug delivery that (A) is independent of the inhalation manoeuvre and (B) is targeted to the correct site in the lung. The purpose of this study is to develop a DPI with an adaptive bypass element that achieves desired drug delivery behaviour.

Computational and experimental methods are used. First, the effect of a generic variable bypass element on entrainment behaviour is modelled. This is done by modelling a DPI as a network of flow. Second, the behaviour of a potential variable bypass element, a flap valve, is studied both computationally and experimentally. Third, the flow resistances are optimized to achieve consistent and desired entrainment behaviour for patients with very different inhalation manoeuvres.

A simulated DPI device design was found that achieves an approximately constant entrainment flow rate of 12 L/min when total flow rates larger than 20 L/min are applied.

The developed DPI is predicted to accurately deliver drug for patients with highly different inhalation manoeuvres.

(188 words)

Keywords

Bypass, Optimization, Flow Control, Entrainment, Dry Powder Inhaler

1 Introduction

Dry powder inhalers (DPIs) are designed for a range of medical, manufacturing and commercial objectives. Possible objectives for DPIs include drug delivery that (A) is independent of the patient's inhalation manoeuvre, and (B) targets the dose to specific regions in the respiratory tract (1,2). To optimize DPIs in accordance with objectives A and B, it is necessary to predict how well a DPI can achieve them, as a function of the DPI geometry and drug powder properties. Computational fluid dynamics (CFD) is a commonly used numerical method in DPI development (3). CFD offers a cost-effective alternative to experimental and clinical studies.

Currently, there is no *passive* DPI on the market which achieves design objective A: deposition independent of inhalation technique (3,4). In passive DPIs the only energy source for powder entrainment and dispersion is the patient's inspiratory flow. While the patient does not have to coordinate actuation and inhalation with a passive DPI, the release of drug $M(t)$ from the device and, consequently, deposition in the lung usually depends strongly on flow rate $Q(t)$ and entrainment geometry. Ideally, the same fraction of drug should deposit in similar pulmonary airways for two patients independent of the applied inhalation flow rate profile $Q(t)$.

Similarly, design objective B, delivery of drug to the target site in the lung, also depends on the inhalation flow rate $Q(t)$ and the entrainment geometry (5). The timing of drug release significantly influences the lung region reached. For example, to treat systemic diseases, such as diabetes or Parkinson's disease, drug delivery to the alveolar region is preferred (3,6,7). For these applications, drug should be released early in the inhalation manoeuvre (an 'early bolus delivery').

The performance of an inhaler with respect to objectives A and B may be influenced by the design. Important considerations include:

- Device entrainment geometry; e.g. entrainment rate for a shear-driven mechanism is typically lower than for a gas-assisted mechanism (8–10).
- Total flow resistance R of the DPI. The inhalation flow rate profile $Q(t)$ of a typical patient is affected by the flow resistance R. Increasing resistance reduces the PIF and thus the rate of drug entrainment.
- Size of a bypass channel. When the size of bypass is increased, while keeping total flow resistance constant, less air flows through the entrainment unit and rate of entrainment usually decreases.

A number of commercially available inhalers incorporate design elements aiming to enhance performance in terms of objectives A and B. For example, *active* DPIs such as Exubera (Pfizer) or Aspirair (Vectura) (11) make use of compressed air. The compressed air provides an additional energy source independent of the patient's lungs. Therefore, good entrainment performance may be achieved independent of the patient (objective A). Other examples include electronically controlled nebulizers, such as the I-neb AAD system (12,13). This device attempts to achieve optimal delivery with a two step process. It first measures patient dependent characteristics such as inspiratory flow rate and length of inhalation manoeuvre. It then uses these measurement to optimally time drug release.

In addition to these active designs some passive DPIs incorporate features to enhance performance. A mechanical component triggers drug release only when a sufficiently high PIF is reached, for example in the Prohaler device (14). This feature prevents patients with low lung function receiving an erroneous dose.

Furthermore, a DPI with a varying bypass flow resistance is briefly mentioned in a patent for a DPI with an integrated reverse flow cyclone chamber for size classification (15). A constant flow through the cyclone element is desired to achieve optimal particle size classification performance (15–17). Harris et al. (15) describe that, in order to keep the flow through the cyclone consistent, the variable bypass resistance must decrease when the inhalation flow rate is large: allowing more air to bypass the cyclone. The patent indicates two potential mechanisms, an 'elastic flap valve' and a 'star valve', that could be used as a variable bypass element. So far, there have been no reports of how such valve concepts could be engineered

into DPI devices, nor have any experimental studies on variable bypass elements in DPIs been published. Currently no DPI on the market uses a variable bypass element.

A variable bypass flow resistance could also be used to keep the flow rate through the entrainment unit more constant. With such an element incorporated in a DPI design, patients with highly different inhalation manoeuvres could potentially achieve more consistent delivery. Such a DPI would automatically adapt the amount of bypass during inhalation to achieve best delivery of drug. Compared to the 'settable bypass' approach proposed in our previous work (18), a single DPI with a variable element could achieve good delivery of drug for a range of different patients without the need to choose the 'correct' amount of bypass. DPIs with a variable (or adaptive) amount of bypass have not been extensively studied in literature. The aim of this study therefore was to design a passive DPI with an adaptive (variable) bypass element that can achieve a (more) consistent and desired entrainment behaviour for patients with very different inhalation manoeuvres. First, the effect of a generic variable bypass element on entrainment behaviour is modelled. Second, the behaviour of a potential candidate bypass element is studied using computational and experimental methods. Finally, the flow resistances in a DPI with a variable bypass element are optimized to achieve desired entrainment behaviour.

2. Methods

2.1 Theory of Flow Resistances

In most DPIs the flow is turbulent and the rate Q proportional to the square root of the applied pressure drop Δp (Darcy–Weisbach equation) (19,20).

$$RQ = \sqrt{\Delta p} \qquad \text{Equation 1}$$

R is the flow resistance of the device. In general, the required breathing power is the product of the flow rate Q and the pressure drop Δp. Note that there may be a variety of airflow paths within a DPI, with not all of the airflow directed through the entrainment compartment (e.g. (21,22)). A DPI may be modelled as a network of flow resistances (23), see Fig. 1a. Such a device consists of three flow resistances R_e, R_b and R_1 . R_e and R_b are the resistances of the entrainment unit and bypass channel, respectively. R_1 is the resistance of any joint inlet or outlet channel, and may, for example, represent the mouth piece (23). In blister-type DPIs (21,22) (a foil sealed drug container is pierced or opened for entrainment) it can be assumed that all other parts of the network have negligible flow resistance. The first two resistances R_e and R_b are in parallel and form an equivalent resistance $R_{e,b}$. R_1 is in series with the other two resistances. The device has a total equivalent flow resistance of R_{tot}.

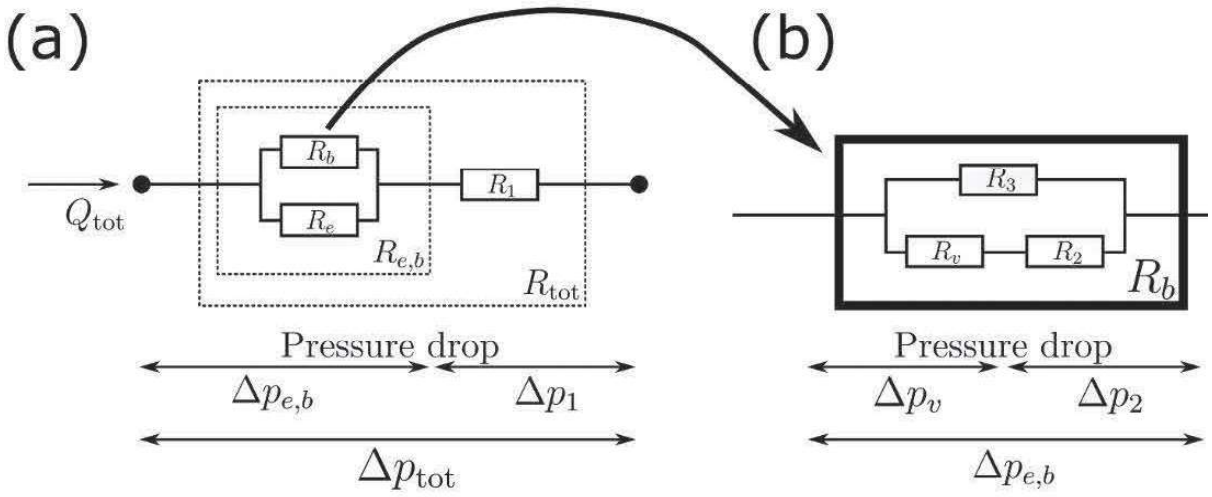

Figure 1: a) Schematic representation of a DPI. R_e and R_b are the flow resistances of the entrainment unit and bypass channel, respectively. Together they form the equivalent resistance $R_{e,b}$. R_1 is a flow resistance in series with $R_{e,b}$. Q_{tot} is the total flow rate through the device. Δp_{tot} is the total pressure drop over the device. $\Delta p_{e,b}$ is the pressure drop over the equivalent flow resistance $R_{e,b}$. Δp_1 is the pressure drop over the resistance R_1. b) Schematic representation of the equivalent circuit to model the bypass flow resistance R_b. R_b is made up of a variable bypass resistance $R_v(\Delta p_v)$ and two constant resistances R_2 and R_3.

The objective is to find an expression for Q_e, the flow rate of air through the entrainment unit, as a function of the total flow rate Q_{tot} or the total pressure drop Δp_{tot}. It is assumed that all flows are in the turbulent regime. Consequently, the relationship between resistance, flow rate and pressure drop are given by Eq. 1:

$$Q_e R_e = Q_b R_b = \sqrt{\Delta p_{e,b}} \qquad \text{Equation 2}$$

$$Q_{\text{tot}} R_1 = \sqrt{\Delta p_1} \qquad \text{Equation 3}$$

Note, since flow resistances R_e and R_b are in parallel, the same pressure drop $\Delta p_{e,b}$ is applied across these resistances. Similarly, the flow rates through the equivalent resistances $R_{e,b}$ and R_{tot} are given by:

$$Q_{\text{tot}} R_{e,b} = \sqrt{\Delta p_{e,b}} \qquad \text{Equation 4}$$

$$Q_{\text{tot}} R_{\text{tot}} = \sqrt{\Delta p_{\text{tot}}} \qquad \text{Equation 5}$$

When a pressure drop is applied across two flow resistances $R_{e,b}$ and R_1 in series, the total pressure drop Δp_{tot} is the sum of the pressure drops across all resistances:

$$\Delta p_{\text{tot}} = \Delta p_{e,b} + \Delta p_1 \qquad \text{Equation 6}$$

$\Delta p_{e,b}$ is the pressure drop across the resistances $R_{e,b}$, and Δp_1 is the pressure drop across resistance R_1.

Furthermore, in a parallel network of flow resistances R_e and R_b, the sum of the flow rates through resistances R_e and R_b is the total flow rate:

$$Q_e + Q_b = Q_{\text{tot}} \qquad \text{Equation 7}$$

By substituting Eq. 2 and 4 into Eq. 7, an equation for the equivalent resistance $R_{e,b}$ may be found:

$$\frac{1}{R_e} + \frac{1}{R_b} = \frac{1}{R_{e,b}} \qquad \text{Equation 8}$$

Similarly, substituting Eq. 3, 4 and 5 into Eq. 6 yields

$$R_{\text{tot}}^2 = R_{e,b}^2 + R_1^2 \qquad \text{Equation 9}$$

Also note, that by eliminating Q_{tot} from Eq. 4 and 5, an equation for $\Delta p_{e,b}$ is found:

$$\sqrt{\Delta p_{e,b}} = \frac{R_{e,b}}{R_{\text{tot}}} \sqrt{\Delta p_{\text{tot}}} \qquad \text{Equation 10}$$

Therefore, recalling Eq. 2 and 5, the flow rate through the entrainment unit is:

$$Q_e = \frac{\sqrt{\Delta p_{e,b}}}{R_e} = \sqrt{\Delta p_{\text{tot}}} \frac{R_{e,b}}{R_e R_{\text{tot}}} \quad = Q_{\text{tot}} \frac{R_{e,b}}{R_e} \qquad \text{Equation 11}$$

In the case of constant flow resistances R_e, R_b and R_1, $R_{e,b}$ and R_{tot} are also constant. Thus, Q_e is proportional to the total flow rate Q_{tot}.

In this study, however, the objective is to analyse the effect of a variable bypass element on the Q_{tot} - Q_e relationship. For this purpose, the bypass flow resistance R_b is modelled as a network of a variable resistance R_v and two constant resistances R_2 and R_3, see Fig. 1b. This choice will facilitate optimisation, and will be explained in more detail in following sections.

Since R_v is a variable bypass element, it does not have a constant value. Instead, R_v is a function of the applied pressure drop Δp_v:

$$R_v = f(\Delta p_v) \qquad \text{Equation 12}$$

The constant flow resistances R_2 and R_3 exist to fine-tune the Q_{tot} - Q_e relationship of the DPI. For example, when R_2 is set to a large value and R_3 is set to a small value, the variable element will have a negligible effect on the DPI. Alternatively, if R_2 is set to a small value and R_3 is set to a large value, the effect of the variable element on the DPI may be extreme.

Analogously to Eq. 8 and 9, the bypass resistance R_b may be expressed in terms of $R_v(\Delta p_v)$, R_2 and R_3:

$$R_b = \left(\frac{1}{R_3} + \frac{1}{\sqrt{R_2^2 + R_v^2(\Delta p_v)}} \right)^{-1} \qquad \text{Equation 13}$$

Similar to Eq. 10, Δp_v can be expressed in terms of $\Delta p_{e,b}$ and resistances $R_v(\Delta p_v)$ and R_2:

$$\sqrt{\Delta p_v} = \frac{R_v(\Delta p_v)}{\sqrt{R_v^2(\Delta p_v) + R_2^2}} \sqrt{\Delta p_{e,b}} \qquad \text{Equation 14}$$

Since R_v depends on the applied pressure Δp_v, the total bypass flow resistance R_b is also pressure dependent. This makes it more difficult to solve Eq. 11, because $R_{e,b}$ and R_{tot} both depend on R_b and hence on the pressure drop. In practice, for any given Δp_{tot}, Eq. 11 may be solved numerically for arbitrary variable resistances $R_v = f(\Delta p_v)$. Once $\Delta p_{e,b}$ is known, Q_e may be evaluated using Eq. 2. By following this approach for a range of different pressure drops, Q_e may be predicted as a function of Δp_{tot} or as a function of Q_{tot}. This approach assumes that the variable bypass element can adapt sufficiently rapidly to changes to the applied pressure. Transient effects are ignored.

As an illustration, Fig. 2 shows how the choice of $R_v(\Delta p_v)$ influences the flow rate Q_e as a function of Δp_{tot} or Q_{tot}. Fig. 2 also shows how the choice of $R_v(\Delta p_v)$ influences the bypass ratio r

$$r = \frac{Q_b}{Q_e} \qquad \text{Equation 15}$$

r is the ratio of air flows through the bypass and the entrainment unit. A constant flow resistance R_v results in linear $\sqrt{\Delta p_{\mathrm{tot}}}$ - Q_e and Q_{tot} - Q_e relationships. The bypass ratio r is constant for a constant flow resistance. For non-constant flow resistance R_v (e.g. 'linear', 'hyperbolic' and 'hyperbolic shifted'), the resulting $\sqrt{\Delta p_{\mathrm{tot}}}$ - Q_e and Q_{tot} - Q_e relationships deviate from linearity. Also, the bypass ratio r is not constant, but grows with total flow rate Q_{tot}. In particular, when the pressure drop $\sqrt{\Delta p_{\mathrm{tot}}}$ and the flow rate Q_{tot} are large, a more constant Q_e is achieved with the variable resistances R_v than with a constant resistance R_v. Note the response when the variable element 'hyperbolic shifted' is used. This element is 'pre-loaded' and has an infinite flow resistance up to a pressure drop $\Delta p_v = 200$ Pa. Consequently, a 'kink' is observed in the $\sqrt{\Delta p_{\mathrm{tot}}}$ - Q_e and Q_{tot} - Q_e-diagrams. The bypass ratio r is zero for flow rates below Q_{tot} ≈ 15 L/min.

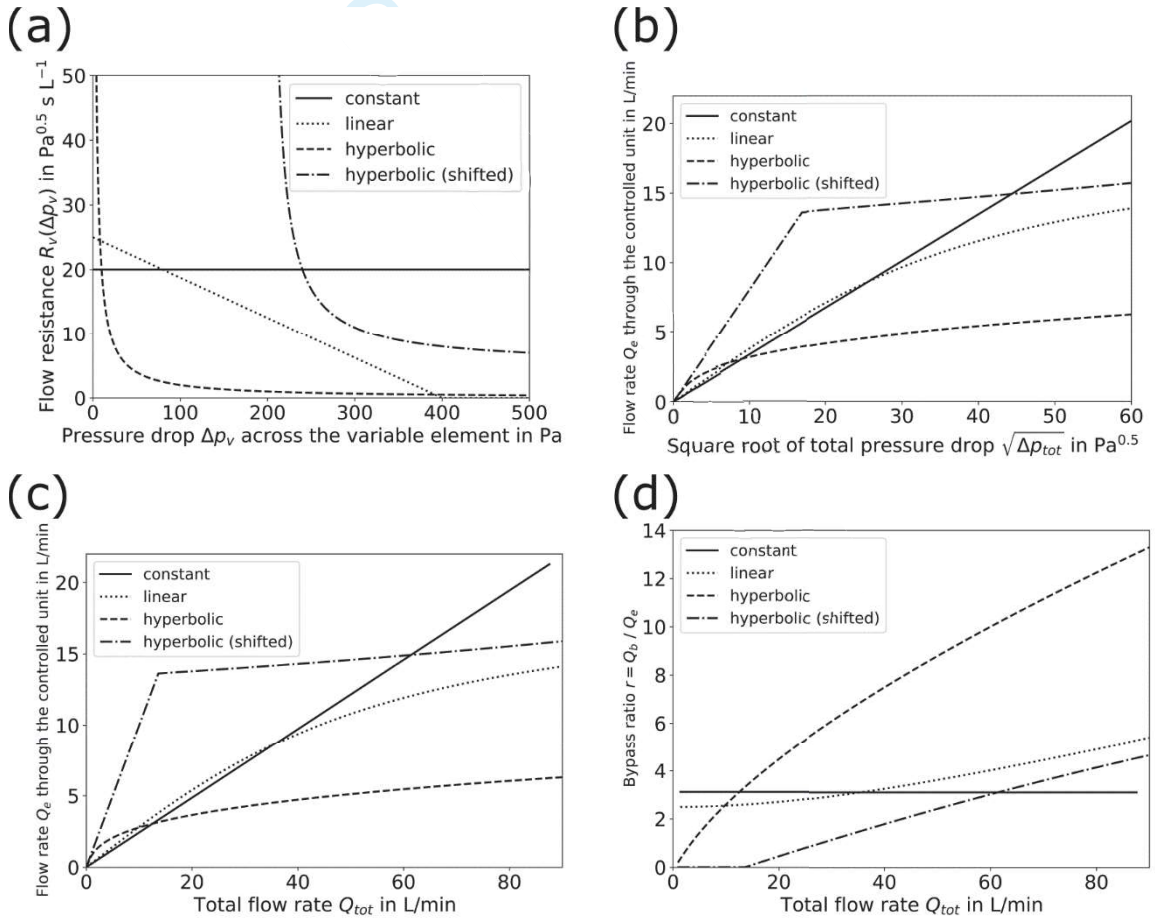

Figure 2: How a variable bypass $R_v(\Delta p_v)$ influences flow through the DPI. $R_e =$ 62.3 Pa$^{0.5}$s L^{-1}, $R_1 =$ 40.6 Pa$^{0.5}$s L^{-1}, $R_2 =$ 0 Pa$^{0.5}$s L^{-1}, $R_3 \rightarrow \infty$. Transient effects ignored: a change of total flow rate Q_{tot} results in immediate response of the bypass element. a)

Four different flow resistance profiles $R_v(\Delta p_v)$. b) Corresponding $\sqrt{\Delta p_{\mathrm{tot}}}$ - Q_e profiles. c) Corresponding Q_{tot} - Q_e profiles. d) Corresponding Q_{tot} - r profiles.

To apply this approach in the design of a real DPI, the dependence of flow resistance R_v and pressure drop Δp_v must be known for a realistic variable bypass element. Thus, a variable bypass element was designed and a fluid-structure interaction (FSI) analysis used to predict $R_v(\Delta p_v)$. The accuracy of the FSI approach was verified experimentally.

2.2 Designing a Variable Bypass Element

2.2.1 Design Considerations for the Variable Bypass Element

A simple 'flap valve' variable bypass element is schematically shown in Fig. 3. The variable element considered is a rigid channel with an integrated, elastically deformable flap. For large applied pressure drops the flap should deform to allow a higher flow rate than would occur otherwise. Initially, the tip of the flap is 'pre-loaded' against the upper boundary of the channel. When a pressure drop is applied across the channel, pressure on the flap's surface pushes it down. Low pressures will be insufficient to overcome the pre-loading. Only for large pressure drops will the flap bend, a gap of size y will then open. The presence of the flap will affect $R_v(\Delta p_v)$, the flow resistance of the element. A potential challenge of this design is that, to eliminate friction, the flap should not touch the channel side walls. Thus, clearance must be maintained which may affect the performance, since air can bypass the flap (a 'leakage'), see Fig. 3b and c. Design dimensions of the variable bypass channel are summarized in the caption of Fig. 3. A detailed understanding of the element's characteristics is required to use it practically in a DPI design. In particular, the relationship between applied pressure drop Δp_v and resulting flow resistance R_v is of interest, see Eq. 12. FSI simulations may be used to investigate the dependence of R_v on Δp_v.

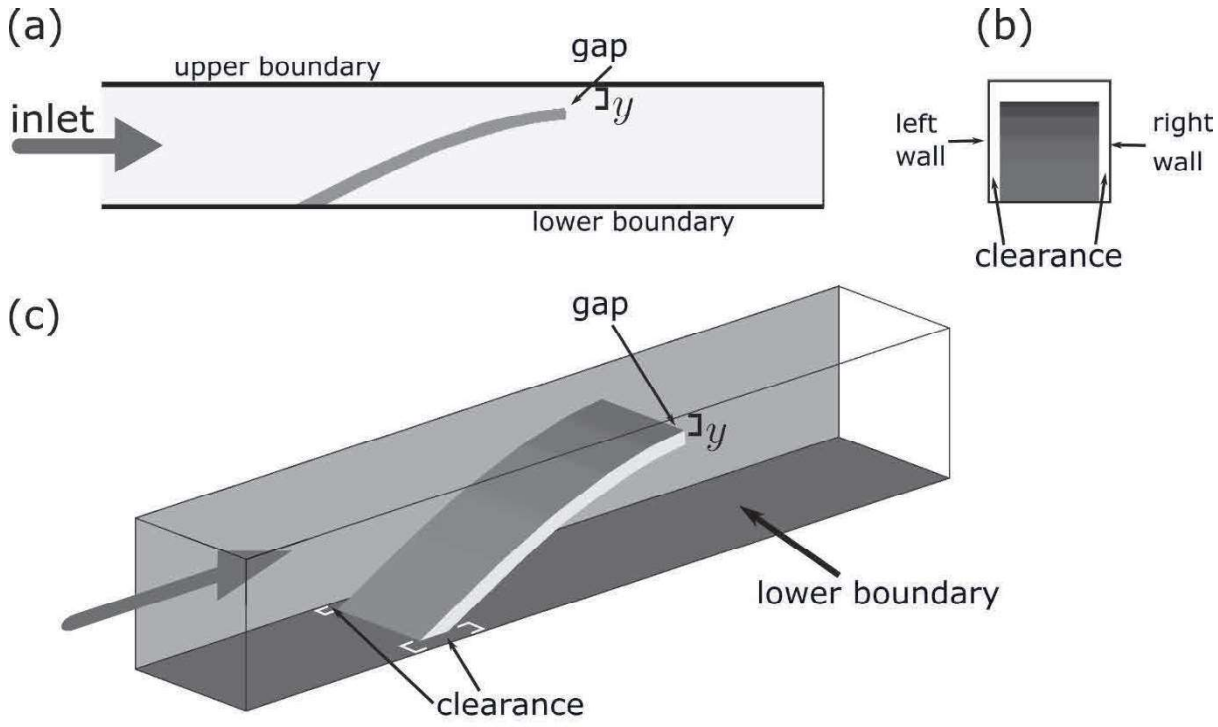

Figure 3: Schematic drawings of a 'flap valve' variable bypass element. The flap is deflected due to a flow. Angle of the flap $\theta = 15°$, flap length $L = 50$ mm, flap thickness $b = 1$ mm, channel width $w_c = 10$ mm, channel depth $d_c = 10$ mm. a) side view, b) end view with clearance between flap and walls indicated c) isometric view

2.2.2 Fluid-Structure Interaction (FSI) Simulation of the Variable Bypass Element

FSI analysis is used to predict how a fluid flow interacts with a deformable structure. In this study FSI analysis was applied to simulate the behaviour of the variable bypass element shown in Fig. 3.

A possible process to solve a FSI problem is:

1. Mesh and model fluid and structure domain.
2. Specify structure-fluid interface, i.e. faces of the fluid and structure in direct contact.
3. Use CFD to predict flow in the fluid domain.
4. Determine stress distribution exerted by the fluid on the deformable structure.
5. Run a structural analysis to predict how the stresses (pressure distribution) deform the structure.
6. Repeat Step 3-5 until results converge.

A commonly used method for Step 5 is finite element analysis (FEA). The last step, i.e. the iteration, is necessary due to the coupling of fluid flow and deformable structure: the fluid flow affects the deformation of the structure, which in turn affects the fluid flow.

In this application a partitioned approach was used (24). The equations governing the fluid flow and the structural deformation are solved with two different solvers. Abaqus (25), a FEA software package, has been used to compute the deformation of the flap. SimpleFOAM, an OpenFOAM (26) solver, was used to solve the fluid flow problem. A Python script (27) was prepared to link both software packages, alternately running OpenFoam CFD simulations and Abaqus FEA jobs.

For simplicity the channel was modelled in two-dimensions only. However, to calculate flow rate through the channel, a width w_c was assumed.

FEA of the flap involved three steps. First, one end was fixed with a zero displacement and rotation constraint. Second, a rigid wall was moved down to pre-load the flap. The vertical distance between the lower end of the flap and the upper boundary was set to d_c, the depth of the channel. Third, a pressure distribution was applied along the flap surface. If the pressure was sufficiently large to overcome the pre-loading, the flap deflected. The deformed shape of the flap was used to update the CFD simulation. In this study, a general purpose quadratic brick element with the reduced integration scheme was chosen. For a two-dimensional beam type geometry this choice may seem over-engineered. However, the goal was to set up a general FSI framework for variable DPI bypass elements, which works for a wide range of different designs. The flap material was polyethylene terephthalate glycol (PETG), a thermoplastic polyester, with properties summarized in Table 1. Table 2 and 3 summarize the CFD and FEA solver settings.

The result of the FSI analysis is the relationship between an applied pressure drop Δp_v and the resulting flow resistance R_v for the chosen variable bypass geometry.

Table 1: Material properties of the elastic flap (28,29).

Property	Value
Material	Polyethylene Terephthalate Glycol (PETG)
Supplier	RS Components (Electrocomponents plc.)
Density ρ_{flap}	1.27 g/cm³
Thickness	1.0 mm
Young's modulus	2.01 - 2.11 GPa
Poisson's ratio	0.37 - 0.44

Table 2: Solver settings for the CFD simulation.

CFD setting	Value
Solver	SimpleFOAM
Size of mesh	0.2 mm globally, but 0.05 mm in the vicinity of the flap

Density of air	1.225 kg/m^3
Dynamic viscosity of air	1.81×10^{-5} kg/(m s)
Turbulence model	k-epsilon
Boundary condition outlet	Atmospheric pressure outlet (0 Pa)
Boundary condition inlet	Velocity inlet (varying magnitude)
Boundary condition wall	No slip
Convergence criterion	1e-06 absolute residual for continuity, x-momentum, y-momentum

Table 3: Solver settings for the Abaqus FEA simulation.

FEA (Abaqus) setting	Value
Mesh	20 x 4 elements
Element type for elastic beam	Reduced integration solid element C3D20R
Steps	1) Set boundary condition: zero displacement and rotation for all nodes on the fixed end ('encastré') 2) Apply wall BC: Move rigid wall into position to pre-load the flap 3) Apply load (pressure distribution)
NLGEOM	On
Interaction	Surface-to-surface contact between wall and flap
Interaction Properties	No friction (frictionless)

2.2.3 Experimental Validation of the FSI Simulation Approach

An experiment was used to validate the FSI simulation. The experiment consisted of a pump, a pressure regulator, a flow meter, an inlet duct, the main unit with the sample flap and an outlet duct, see Fig. 4. The main unit was made of transparent acrylic, so deformation of the sample material could be observed. Pressure drop, flow rate and the size of the gap between flap and upper boundary y were measured simultaneously. Photographs of the deflected flap allowed a qualitative comparison between experiment and FSI simulation. The inlet duct had static pressure taps to measure the pressure differential between a point 70 mm upstream of the flap and atmospheric pressure with a manometer. The inlet duct also helped to fully condition the flow. The main purpose of the outlet duct was to guide the flow away from the main unit and the camera. The flap was an 8 mm wide PETG strip. The channel width was 10 mm, giving a clearance of 1 mm on each side, see Fig. 3.

Q_{free}, the flow rate through the bypass channel when the flap was 'free' to move was recorded for a range of pressure drops Δp_v. Flow occurred even when Δp_v was small and the flap touched the upper boundary due to airflow through the clearance as indicated in Fig. 3. To quantify this leakage, a second set of experiments was conducted with the tip of the flap glued to the upper boundary. Q_{fixed}, the flow rate through the bypass channel when the flap was 'fixed' (i.e. glued to the upper boundary), was recorded as a function of Δp_v.

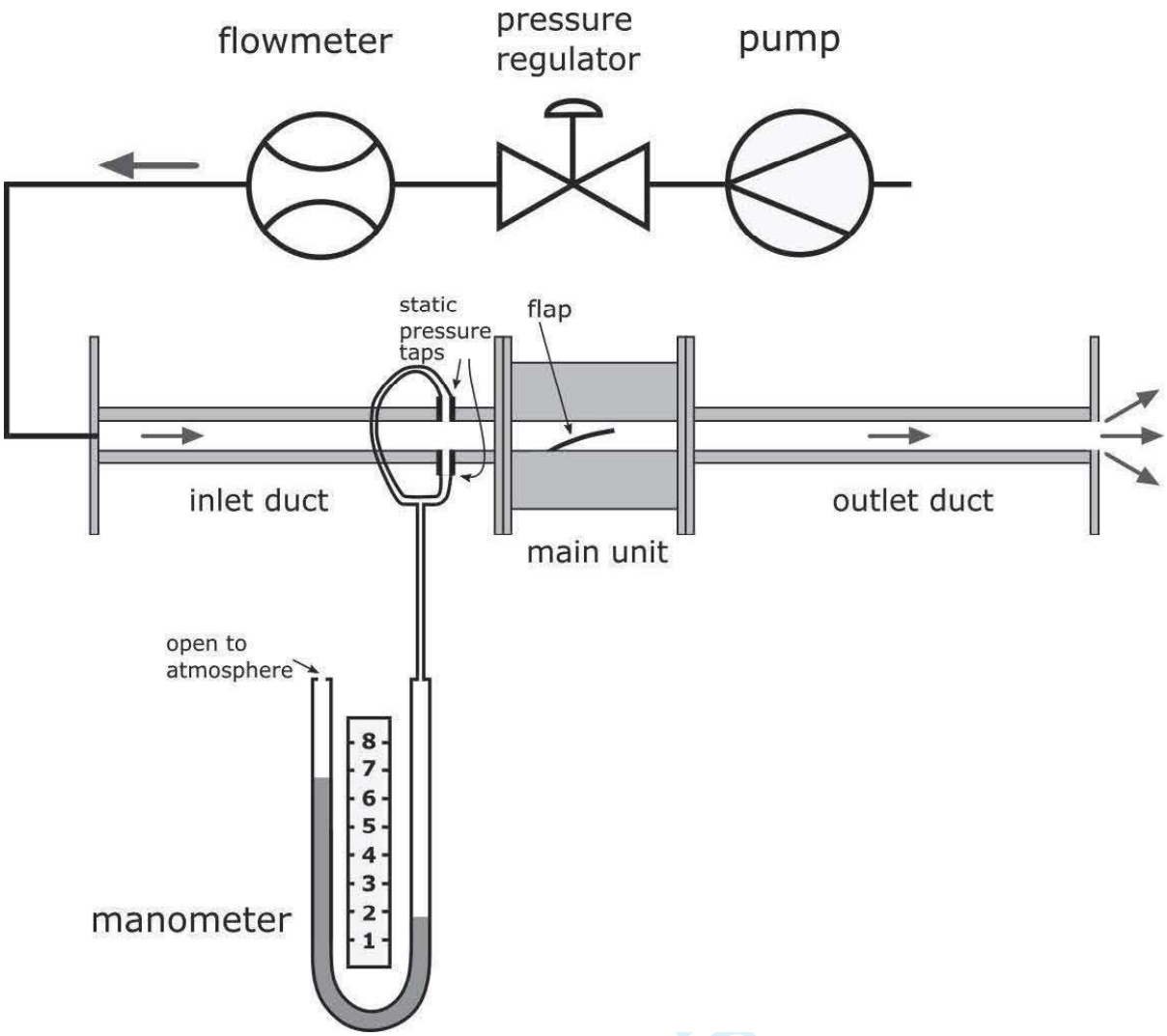

Figure 4: Experimental setup to measure the response of the variable bypass element: Air flows through the main unit with a sample flap. Flowrate, pressure drop and flap deflection are measured.

2.3 Modelling the Rate of Drug Release

To optimize DPIs it is important to understand how the inhalation flow rate $Q_e(t)$ and entrainment geometry affect the rate of drug release. In previous work (30), we applied multiphase CFD to predict *M(t)*, the mass of drug powder released as a function of time *t* from a DPI entrainment geometry. This method was successfully validated by comparing CFD predictions to experimental measurements (10). While this method can predict *M(t)* accurately, it is computationally inefficient. Consequently, in previous work, we developed an efficient meta-model (18). Using a small number of computationally expensive CFD simulations, a low fidelity model was constructed that can make additional predictions with low

computational cost. The meta-model was validated with results from additional CFD simulations. In this study the meta-model was used to predict *M(t)* depending on applied inhalation flow rate profile $Q_e(t)$. Fig. 5 shows the entrainment geometry used.

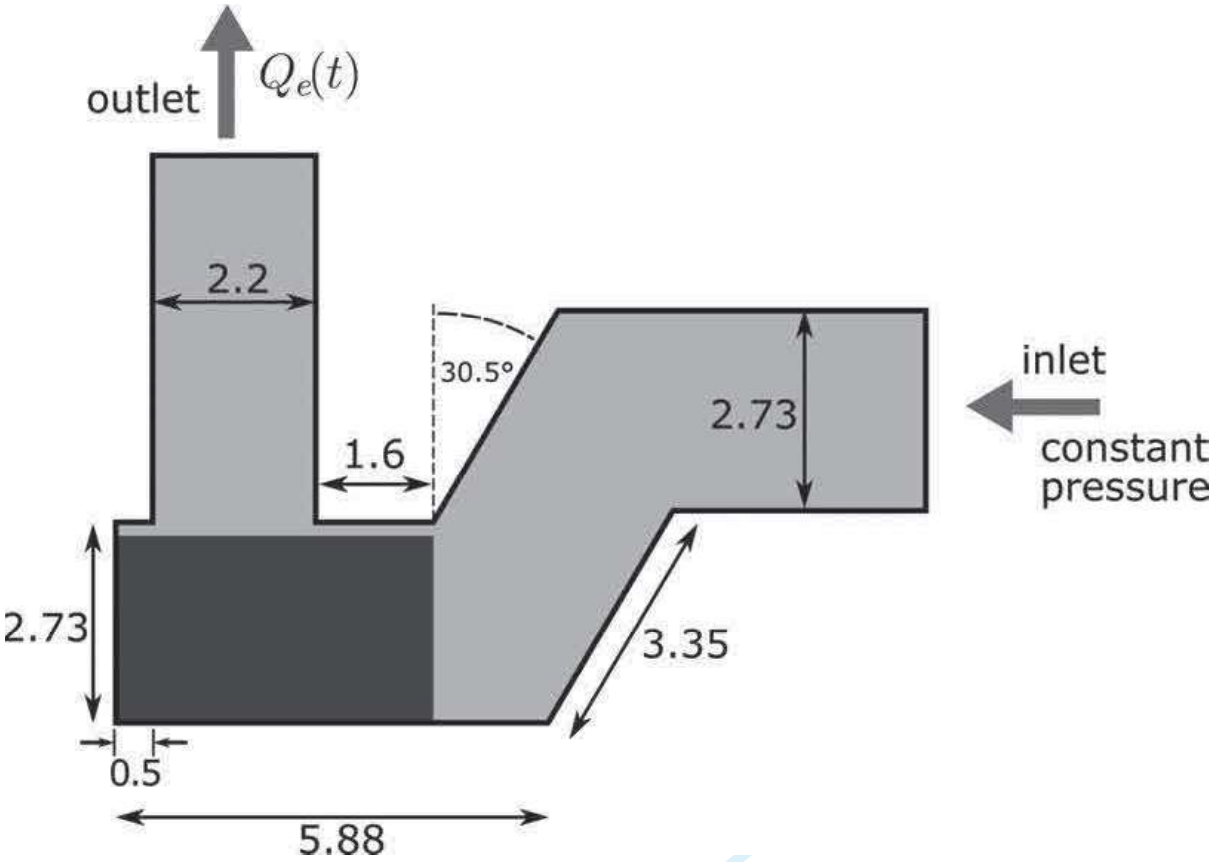

Figure 5: Entrainment geometry used in this study (dimensions in mm). This is one of the optimized entrainment geometries found in Kopsch (31). Area shaded in dark grey represents the initial distribution of drug powder.

2.4 Optimization Framework

The device layout considered in this study is shown in Fig. 1. It consists of an entrainment unit with constant flow resistance R_e, a bypass element R_b and another constant flow resistance R_1. The bypass resistance R_b is modelled as a network of two constant resistances R_2 and R_3 and the variable resistance R_v (Δp_v). Therefore, given a specific variable bypass resistance $R_v(\Delta p_v)$, the whole device layout may be described by a vector of design variables given by:

$$\mathbf{x} = (R_e, R_1, R_2, R_3) \qquad \text{Equation 16}$$

The objective is to design a DPI that achieves drug delivery that is (A) patient independent and (B) similar to a desired target profile. As in our previous work (30) two cost functions C_A and C_B are used to quantify performance. C_A measures the similarity of drug release with different inhalation profiles, C_B compares release to a target function (shown in Fig. 10a and 11). It is hoped that this variable bypass DPI performs with different inhalation profiles better than classical DPIs with constant bypass elements. Therefore, two extreme inhalation profiles $T_{\mathrm{tot},1}$ and $T_{\mathrm{tot},2}$ (Fig. 6) were chosen to calculate the cost function C_A. Profiles T_1 and T_2 have a PIF of 100 L/min and 25 L/min, respectively. A DPI design that works with these extreme profiles should perform well with less extreme flows.

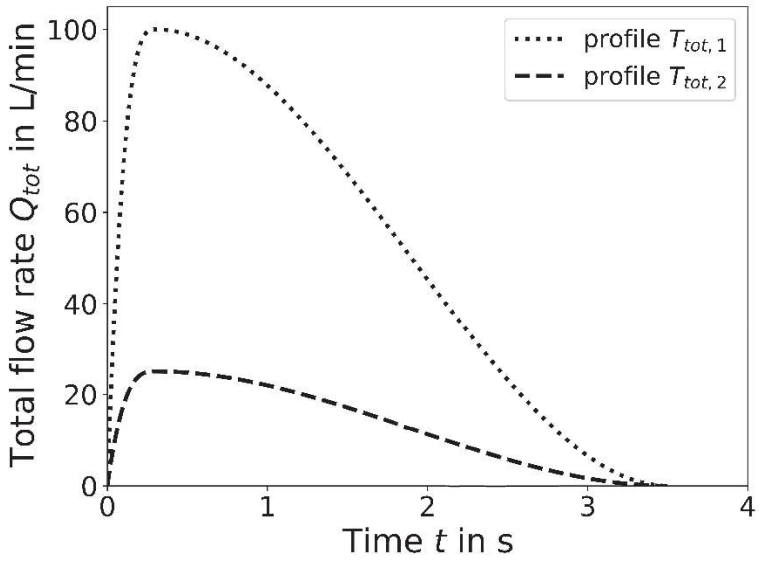

Figure 6: Two extreme flow rate profiles $T_{\mathrm{tot},1}(t)$ and $T_{\mathrm{tot},2}(t)$.

A gradient descent optimization algorithm (32) was used to minimize a combined cost function $C = C_A + C_B$ by iteratively varying the design vector $\mathbf{x} = (R_e, R_1, R_2, R_3)$. In each iteration:

i) the method described in Section 2.1 was used to predict Q_e, the flow rate through the entrainment unit, as a function of Q_{tot} for the current design vector **x** ;

ii) once the Q_{tot} - Q_e relationship is known, the meta-model (Section 2.3) was used to predict $M(x)$ (mass of drug released as a function of scaled volume) for the two inhalation profiles $T_{\mathrm{tot},1}(t)$ and $T_{\mathrm{tot},2}(t)$;

iii) the value of the cost function $C = C_A + C_B$ was calculated.

Iterations were repeated until C converged on a minimum.

Note that the scaled volume x is the fraction of inhaled volume of air to maximum lung volume. The reason for expressing M, the mass of released drug, in terms of x is that the region of pulmonary drug deposition depends on when the drug is released with respect to the inhaled volume (33,34).

Finally, the quality of the optimized device has been evaluated by testing it for a range of realistic inhalation profiles.

3 Results

3.1 Comparison of FSI Simulations and Experiments

Fig. 7a and b show contour plots of static pressure when flow rates $Q = 18.2$ L min^{-1} and $Q = 43.2$ L min^{-1} are applied. These flow rates were chosen to give a gap between the upper boundary and flap of 1 mm and 2 mm, respectively. In both cases the static pressure reaches a value close to zero a few centimeters downstream of the flap. Fig. 7b and c show contour plots of velocity magnitude for the same flow rates; the flow accelerates in the narrow gap between flap and upper boundary.

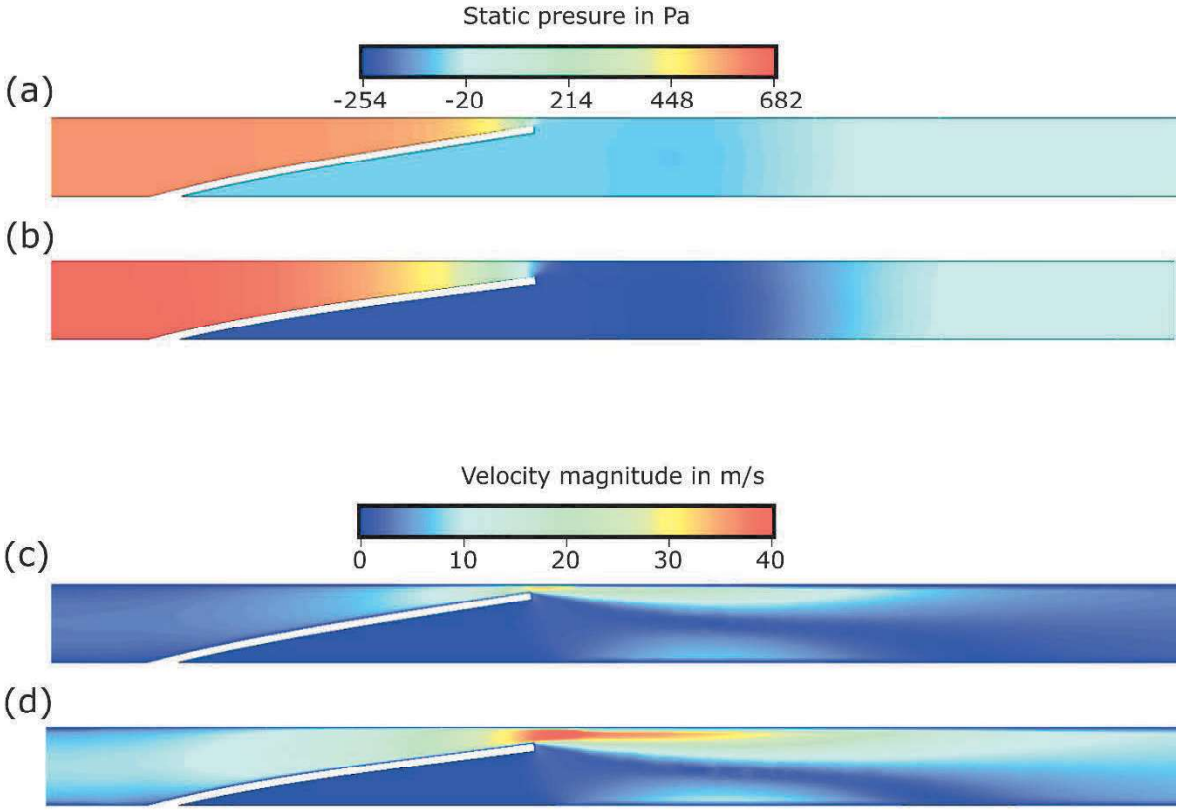

Figure 7: Contour plots of the static pressure: a) $Q = 18.2$ L min^{-1} ($y = 1$ mm) b) $Q = 43.2$ L min^{-1} ($y = 2$ mm). Contour plots of the velocity magnitude: c) $Q = 18.2$ L min^{-1} d) $Q = 43.2$ L min^{-1}.

Fig. 8 is a qualitative comparison of computational FSI results and experiment. Initially, when no pressure drop is applied, the variable bypass element is closed and no flow is observed. When the pressure drop is increased to 400 Pa the element remains closed due to the pre-loading of the flap. At 550 Pa the element starts to open. After a change of applied pressure the flap moved quickly to a new stable position; the flap did not vibrate for the range of pressure drops tested.

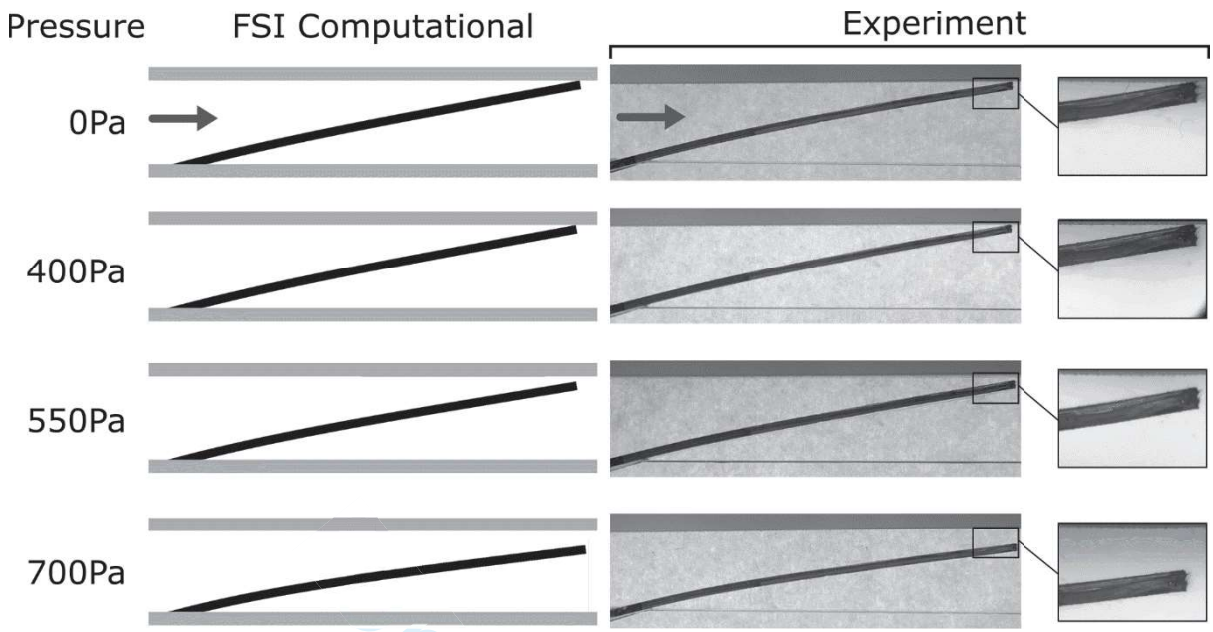

Figure 8: Qualitative comparisons of computational and experimental results for the variable bypass element. Columns show the FSI simulation results, photos from the experiment and detail photos of the flap tip. Rows correspond to different pressure drops.

Quantitative results are shown in Fig. 9. Fig. 9a shows the flowrate as a function of pressure drop when the flap is free to move (Q_{free}) and when it is fixed (glued) to the upper boundary (Q_{fixed}). For pressure drops smaller than 450 Pa similar flow rates are observed for Q_{free} and Q_{fixed}. For these pressure drops the flap is in contact with the upper boundary, even when free to move. For larger pressure drops the measurements for Q_{free} and Q_{fixed} deviate: larger flow rates are observed for Q_{free}, i.e. when the flap is free to open. These results show the leakage through the clearance at the sides of the flap (Fig. 3). The two-dimensional FSI model does not account for this leakage. However, the real variable bypass element may be approximated as an ideal variable element with perfect sealing together with a constant flow resistance in parallel to model the leakage. With this model in mind the flowrate through the ideal variable element is approximately Q_{free} - Q_{fixed}. Therefore, Fig. 9b compares the computational result for the pressure-flowrate relationship from the 2D FSI simulation with the measurement Q_{free} - Q_{fixed}. Good agreement is observed. Fig. 9c plots y, the size of gap between flap and upper boundary, as a function of pressure drop. Good agreement is again observed; experiment and simulation both predict that the flap opens at a pressure drop of around 450 Pa. Fig. 9d is a plot of the flow resistance R_v of the simulated variable bypass element as a function of pressure drop Δp_v, see Eq. 12. For the ideal variable bypass device no flowrate is observed for pressure drops less than 450 Pa and the flow resistance therefore becomes infinitely large.

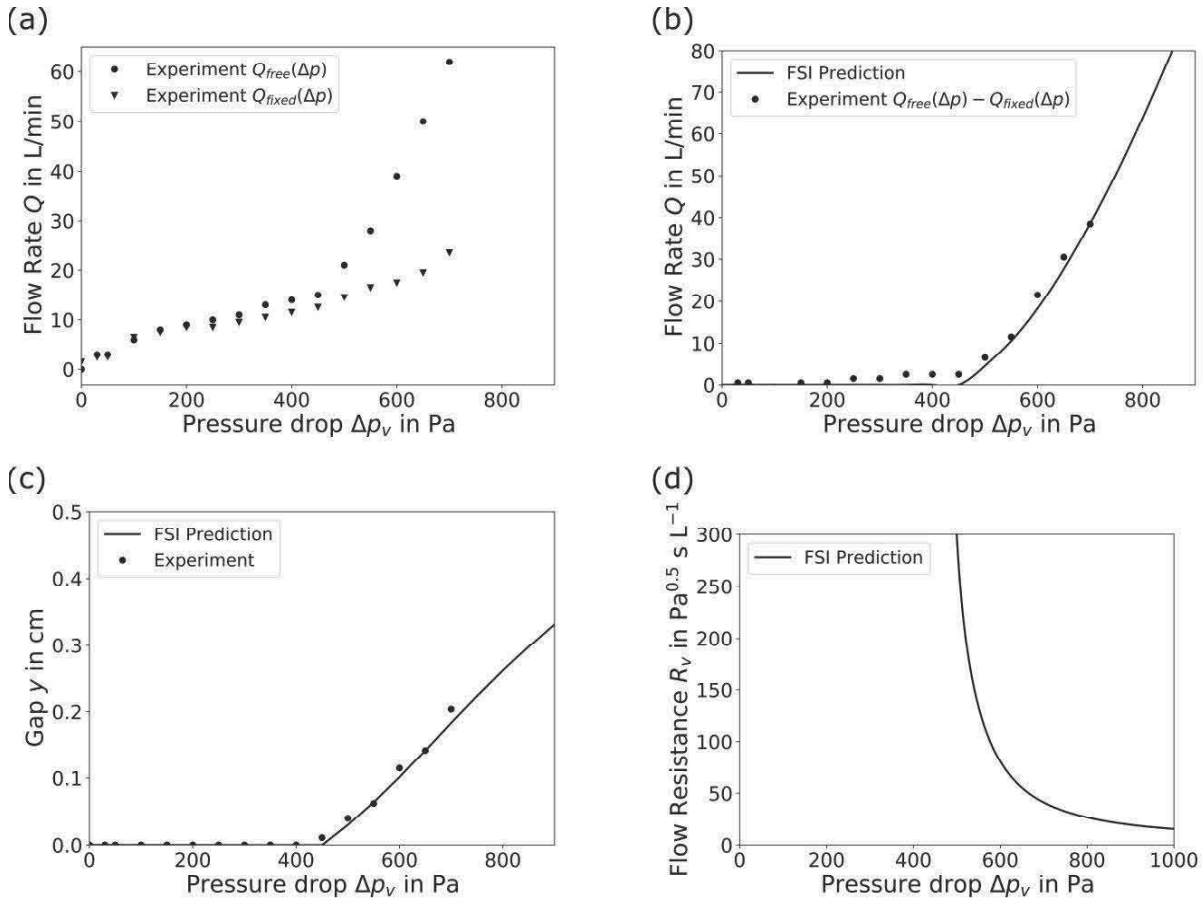

Figure 9: a) Experimental results for flow rate as a function of applied pressure drop Δp_v when the flap is free to move (Q_{free}) and the leakage flow when it is fixed (Q_{fixed}). b) Comparison of predicted flowrate and experimental flowrate difference Q_{free} - Q_{fixed}. c) Comparison of computational and experimental results for the gap size y. d) Flow resistance R_v of the bypass element as a function of applied pressure drop Δp_v.

3.2 Optimization Results

The simulated variable flow resistance R_v was used in a network of flow resistances to achieve optimal drug delivery in terms of the overall cost function $C = C_A + C_B$ for two extreme inhalation profiles $T_{\text{tot},1}(t)$ and $T_{\text{tot},2}(t)$, see Fig. 6. The optimal values for the flow resistances are shown in Table 4.

Table 4: Optimized values of the design variables.

Design variable	Optimized value in $Pa^{0.5} s L^{-1}$
R_e	113.3
R_1	70.9
R_2	3.0
R_3	208.1

Fig. 10a shows $M(x)$, the mass of released drug as a function of scaled volume x, for the two inhalation profiles $T_{tot,1}$ and $T_{tot,2}$ together with the target profile M_{target}. Including the variable element helps to achieve good agreement with the target profile (cost function B) and breath rate independence (cost function A), even though $T_{tot,1}$ and $T_{tot,2}$ are very different.

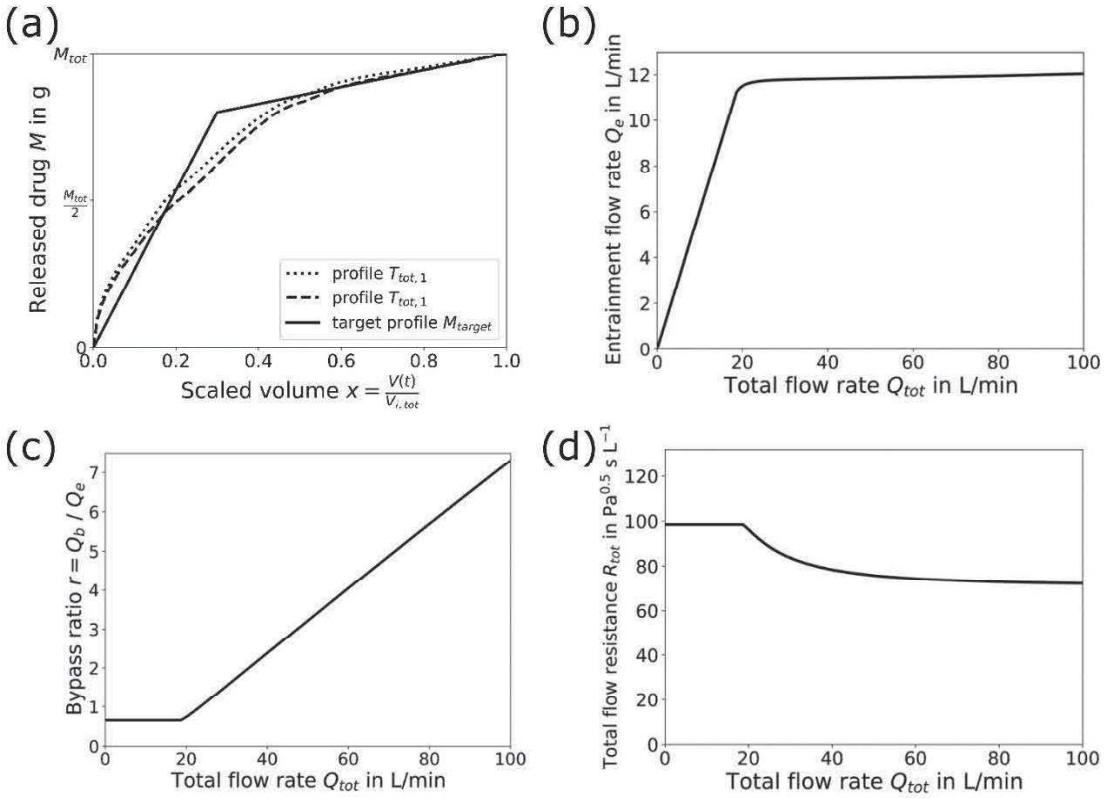

Figure 10: a) Drug release profiles $M(x)$ for an optimized DPI with variable bypass element for two extreme inhalation profiles $T_1(t)$ and $T_2(t)$. Behaviour of the idealized, optimized DPI: b) Q_e, flow rate through the entrainment unit, as a function of Q_{tot}, total inhalation flow rate. c) $r = \frac{Q_b}{Q_e}$, bypass ratio, as a function of Q_{tot}. d) R_{tot}, total flow resistance, as a function of Q_{tot}.

Fig. 10b, c and d display the response of the optimized DPI. Fig. 10b shows the Q_{tot} - Q_e relationship. For total flowrates larger than $20\ \text{L/min}$ an almost constant entrainment flow rate Q_e is observed. Since the rate of drug entrainment mainly depends on the flow rate in the entrainment compartment the release rate should be very similar for different patients. Fig. 10c shows the bypass ratio *r* as a function of total inhalation flow rate Q_{tot}. A small constant bypass ratio is observed for Q_{tot} smaller than 20 L/min. For Q_{tot} larger than 20 L/min, the bypass ratio starts to grow approximately linearly. Fig. 10d is the total flow resistance R_{tot} as a function of Q_{tot}.

To test the optimized variable bypass DPI, performance was evaluated using the same sample inhalation profiles as used in our previous paper (18) on a DPI with a settable bypass, see Fig. 11. Fig. 11a and b show inhalation manoeuvres of two sample patients with different lung function. Fig. 11c and d show the corresponding entrainment flow rate profiles $Q_e(t)$. Since the Q_{tot} - Q_e profile reaches a plateau of $Q_e \approx 12\ \text{L/min}$ when the total flow rate $Q_{\text{tot}} \geq 20\text{L/min}$, these profiles appear as if they are 'cut off'. Fig. 11e and f show the corresponding drug release profiles *M(x)*. Good agreement with the target profile is observed for both patients. This DPI achieves a similar performance to the concept DPI proposed in our previous work where the resistance could be set at a fixed magnitude chosen to be appropriate for an individual patient's lung function (18). However, the advantage of this variable resistance DPI is that it can work for a large range of patients with different inhalation profiles, without the requirement for patient dependent personalization.

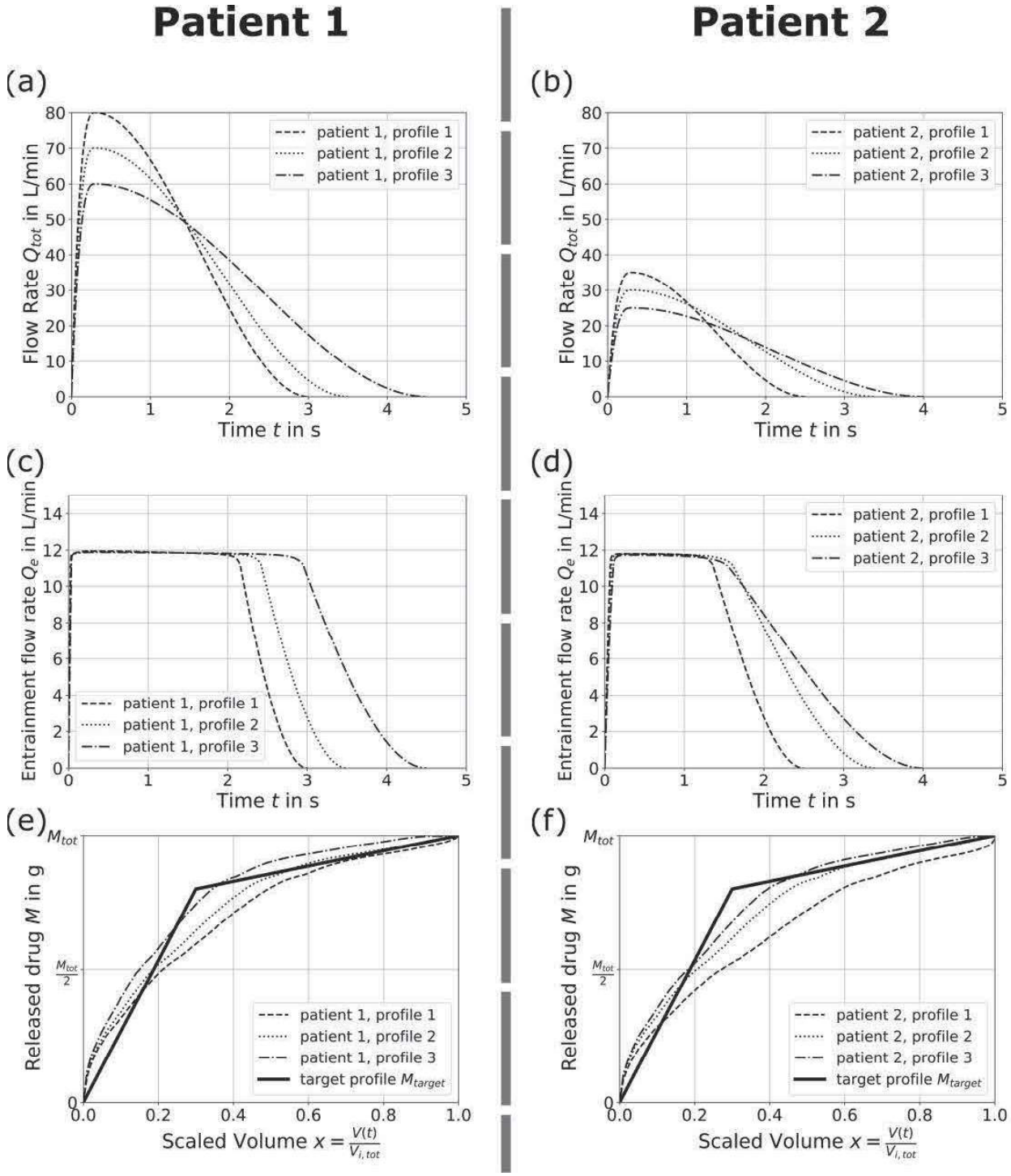

Figure 11: Illustrative inhalation profiles: a) Patient 1, with normal lung function; b) Patient 2, with reduced lung function. The corresponding entrainment flow rate profiles c) Patient 1, d) Patient 2. Corresponding drug release profiles e) Patient 1, f) Patient 2.

4 Conclusions

In this study numerical simulations and optimization techniques were applied to design a DPI with a variable, adaptive bypass channel. Computational FSI and experiments have been applied to understand the response of a simple, idealized flap valve variable bypass. This element was utilized to achieve a more constant flow rate through the entrainment unit than would be possible with fixed flow resistances. The developed DPI is predicted to accurately deliver drug for patients with highly different inhalation manoeuvres without the need to choose the correct amount of bypass for each patient. The effectiveness of the optimized DPI has been shown by means of a numerical study.

5 Funding Statement

TK was funded by an EPSRC PhD studentship (EP/M506485/1). DM was funded by an EPSRC Manufacturing the Future award (EP/N025075/1).

6 References

1. Virchow JC, Crompton GK, Dal Negro R, Pedersen S, Magnan A, Seidenberg J, et al. Importance of inhaler devices in the management of airway disease. Respir Med. 2008;102(1):10–9.
2. O'Connor BJ. The ideal inhaler: Design and characteristics to improve outcomes. Respir Med. 2004;98:10–6.
3. Licalsi C, Christensen T, Bennett J V., Phillips E, Witham C. Dry powder inhalation as a potential delivery method for vaccines. Vaccine. 1999;17(13–14):1796–803.
4. Muralidharan P, Jr DH, Mansour HM. Dry powder inhalers in COPD, lung inflammation and pulmonary infections. Expert Opin Drug Deliv. 2017;5247.
5. Bäckman P, Adelmann H, Petersson G, Jones CB. Advances in inhaled technologies: Understanding the therapeutic challenge, predicting clinical performance, and designing the optimal inhaled product. Clin Pharmacol Ther. 2014;95(5):509–20.
6. Laube BL. The expanding role of aerosols in systemic drug delivery, gene therapy and vaccination: an update. Transl Respir Med. 2014;2(1):3.
7. Scheuch G, Kohlhaeufl MJ, Brand P, Siekmeier R. Clinical perspectives on pulmonary systemic and macromolecular delivery. Adv Drug Deliv Rev [Internet]. 2006 Oct;58(9–10):996–1008. Available from: http://linkinghub.elsevier.com/retrieve/pii/S0169409X0600144X
8. Dunbar CA, Hickey AJ, Holzer P. Dispersion and characterisation of phamaceutical dry powder aerosols. Kona. 1998;16(16):7–45.
9. Daniher DI, Zhu J. Dry powder platform for pulmonary drug delivery. Particuology. 2008;6:225–38.
10. Tuley R, Shrimpton J, Jones MD, Price R, Palmer M, Prime D. Experimental observations of dry powder inhaler dose fluidisation. Int J Pharm. 2008;358(1–2):238–47.
11. Hoppentocht M, Hagedoorn P, Frijlink HW, de Boer AH. Technological and practical challenges of dry powder inhalers and formulations. Adv Drug Deliv Rev. 2014;75:18–31.
12. Nikander K, Prince I, Coughlin S, Warren S, Taylor G. Mode of breathing-tidal or slow and deep-through the I-neb Adaptive Aerosol Delivery (AAD) system affects lung deposition of (99m)Tc-DTPA. J Aerosol Med Pulm Drug Deliv. 2010;23 Suppl 1:S37–43.

13. Geller DE, Kesser KC. The I-neb adaptive aerosol delivery system enhances delivery of alpha1-antitrypsin with controlled inhalation. J Aerosol Med Pulm Drug Deliv. 2010;23 Suppl 1:S55–9.
14. Mitra AK, Kwatra D, Vadlapudi AD. Drug delivery. Jones and Bartlett Publishers, Inc; 2014.
15. Harris DS, Smith SJ. Patent US 8,261,739 B2 - Dry Powder Inhalers. Patent. US 8,261,739 B2, 2012.
16. Cheng SJ. Numerical and Experimental Study of Cyclone Separators for Aerosol Drug Delivery. University of Cambridge; 2012.
17. Parisini I, Cheng SJ, Symons D, Murnane D. Potential of a cyclone prototype spacer to improve in vitro dry powder delivery. Pharm Res. 2014;31(5):1133–45.
18. Kopsch T, Murnane D, Symons D. A personalized medicine approach to the design of dry powder inhalers: Selecting the optimal amount of bypass. Int J Pharm. 2017;529(1–2):589–96.
19. de Koning JP. Dry Powder Inhalation, Technical and Physiological Aspects, Prescribing and Use. University of Groningen; 2001.
20. Shames IH. Mechanics of fluids. McGraw-Hill; 2003.
21. Shur J, Saluja B, Lee S, Tibbatts J, Price R. Effect of Device Design and Formulation on the In Vitro Comparability for Multi-Unit Dose Dry Powder Inhalers. AAPS J. 2015;
22. Grant AC, Walker R, Hamilton M, Garrill K. The ELLIPTA Dry Powder Inhaler: Design, Functionality, In Vitro Dosing Performance and Critical Task Compliance by Patients and Caregivers. J Aerosol Med Pulm Drug Deliv. 2015;28(6):474–85.
23. Ertunç Ö, Köksoy Ç, Wachtel H, Delgado A. A method for the aerodynamic design of dry powder inhalers. Int J Pharm. 2011;416:25–34.
24. Bungartz H-J, Mehl M, Schäfer M, editors. Fluid Structure Interaction II. Springer-Verlag Berlin Heidelberg; 2010.
25. Simulia (Dassault Systèmes Simulia Corp.). Abaqus 6.12 User's Manual [Internet]. 2012. Available from: http://www.maths.cam.ac.uk/computing/software/abaqus_docs/docs/v6.12/pdf_books/GET_STARTED.pdf
26. OpenFOAM Foundation. OpenFOAM 2.4 [Internet]. 2016 [cited 2016 Feb 15]. Available from: http://www.openfoam.org/
27. Python Software Foundation. Python language reference, Version 2.7.6 [Internet]. 2016. Available from: https://docs.python.org/2/reference/
28. RS Components Ltd. Datasheet: Polyethylene Terephthalate Glycol Sheet (Stock Number: 334-6444) [Internet]. 2017 [cited 2017 Oct 15]. Available from: http://docs-europe.electrocomponents.com/webdocs/1580/0900766b81580523.pdf
29. Dielectric Corporation. PETG, General material properties [Internet]. 2017 [cited 2017 Oct 15]. Available from: http://www.dielectriccorp.com/downloads/thermoplastics/petg.pdf
30. Kopsch T, Murnane D, Symons D. Optimizing the entrainment geometry of a dry powder inhaler: Methodology and preliminary results. Pharm Res. 2016;33(11):2668–2679.
31. Kopsch T. Computational Modelling and Optimization of Dry Powder Inhalers. University of Cambidge; 2018.
32. Nocedal J, Wright SJ. Numerical optimization. Springer; 2006. (Springer Series in Operations Research and Financial Engineering).
33. Brand P, Häußinger K, Meyer T, Scheuch G, Schulz H, Selzer T, et al. Intrapulmonary distribution of deposited particles. J Aerosol Medice. 1999;12(4):275–84.
34. Heyder J, Blanchard JD, Brain JD. Particle deposition in volumetric regions of the human respiratory tract. Ann Occup Hyg. 1988;32:71–9.